# Reverse Monte Carlo studies of $CeO_2$ using neutron and synchrotron radiation techniques

OPEN ACCESS
IOP Publishing | Royal Swedish Academy of Sciences Physica Scripta
Phys. Scr. **92** (2017) 034002 (9pp) https://doi.org/10.1088/1402-4896/aa547f

# Reverse Monte Carlo studies of $CeO_2$ using neutron and synchrotron radiation techniques

**Adam H Clark[1], Huw R Marchbank[1], Timothy I Hyde[2], Helen Y Playford[3], Matthew G Tucker[3,4,5] and Gopinathan Sankar[1]**

[1] Department of Chemistry, University College London, 20 Gordon Street, London WC1H 0AJ, United Kingdom
[2] Johnson Matthey Technology Centre, Blount's Court, Sonning Common, Reading RG4 9NH, United Kingdom
[3] ISIS Facility, Rutherford Appleton Laboratory, Chilton, Didcot, Oxon OX11 0QX, United Kingdom
[4] Diamond Light Source, Harwell Science and Innovation campus, Didcot, Oxon, OX11 0DE, United Kingdom

E-mail: g.sankar@ucl.ac.uk

Received 3 August 2016, revised 30 November 2016
Accepted for publication 19 December 2016
Published 31 January 2017

**Abstract**

A reverse Monte Carlo analysis method was employed to extract the structure of $CeO_2$ from Neutron total scattering (comprising both neutron diffraction (ND) and pair-distribution functions (PDF) and Ce $L_3$- and K-edge EXAFS data. Here it is shown that there is a noticeable difference between using short ranged x-ray absorption spectroscopy data and using medium-long range PDF and ND data in regards to the disorder of the cerium atoms. This illustrates the importance of considering multiple length scales and radiation sources.

Supplementary material for this article is available online

Keywords: reverse Monte Carlo, ceria, neutron total scattering, EXAFS

(Some figures may appear in colour only in the online journal)

## Introduction

Ceria has numerous important applications due to the interesting chemistry of the cerium atoms. In contrast to the other lathanides, Ce can lose a 4f electron, resulting in an electron configuration of [Xe] $5d^1$ $6s^2$. In ceria, this facilitates the reduction of cerium atoms and the release of oxygen. Furthermore this allows the re-oxidation of cerium atoms (which is enhanced by the fluorite structure). The ability to undergo reduction–oxidation means ceria is used extensively for a range of applications, in particular emission based catalytic control [1–5].

Non-stoichiometry of ceria, which involves reduction of cerium and removal of oxygen and produces vacancies in the structure, can be induced by certain synthetic methodologies [6]. Vacancies are likely to increase the amount of disorder within the structure and therefore understanding the structure of highly crystalline, fully stoichiometric $CeO_2$ is crucial in relating to its reactivity and properties.

Methods such as lab based x-ray diffraction, are used regularly in the characterisation of ceria, though each technique only provides insight into certain structural ranges within the material, so only by combining numerous methods will a full understanding of the properties of the short, medium and long range structure be obtained. Neutron diffraction (ND) based methodologies are appropriate for ceria due to the

[5] Current address: Spallation Neutron Source, One Bethel Valley Road, MS-6475, Oak Ridge, TN 37831-6475, USA.

relatively similar neutron scattering cross sections for Ce and O [7] (in contrast to x-ray scattering which is dominated by the more massive Ce atoms) [8]. Utilising rietveld refinement [9] and PDF analysis, it has been shown that interstitial oxygen defects can be present in the system, showing oxide ions can be highly mobile within the ceria fluorite structure. Although diffraction techniques are powerful in understanding the long-range bulk structure, many differences in the short and medium range order may be missed by these techniques. Therefore, making use of local structural technique, in particular x-ray absorption spectroscopy as it is element specific and sensitive to local structural changes, is clearly an advantage. The use of PDF, obtained from total scattering data, is a useful complementary technique as this simultaneously can show the short, medium and long range structure in contrast to x-ray absorption spectroscopy (XAS) and standard diffraction methods. Whilst the data from these techniques can be analysed independently, it is necessary to further the analysis procedure to combine these methodologies to attain a more thorough understanding of the materials. Reverse Monte Carlo (RMC) appears to be a method which can provide such possibility as any of these data sets can be analysed using RMC based suite of programs. Here we report the use of RMC methods to extract the structure of a crystalline $CeO_2$.

## Experimental

### *Sample preparation*

A $CeO_2$ diffraction standard (674b) was obtained from National Institute of Standards and Technology (NIST).

### *Neutron total scattering*

Total scattering patterns were obtained on the POLARIS [10] instrument based at the ISIS Facility, Rutherford Appleton Laboratory, UK. The sample was ground and placed in a cylindrical vanadium foil can (internal diameter = 8 mm). Data were collected for six hours. Measured data from each of the five detector banks were initially processed using MantidPlot [11] to obtain powder diffraction patterns.

### *XAS at Ce $L_3$-edge and Ce K-edge*

XAS data was obtained at the Ce $L_3$-edge (5723.4 eV) at ambient conditions on the BM26A beam line [12], European Synchrotron Research Facility (ESRF) operating at 6 GeV and current of 100 mA. Data was collected in transmission mode using ionisation chambers and a Si (111) double crystal monochromator. Roughly 10 mg of the ceria material was ground with circa 90 mg of fumed silica and pressed into a pellet. XAS data was measured in step scans between 5623.0 and 6154.0 eV. XAS data was obtained at the Ce K-edge (40443 eV) at ambient conditions on the BM23 beam line [13], ESRF. Data was collected in transmission mode using ionisation chambers and a Si (311) double crystal monochromator. About 95 mg of sample was mixed and ground with approximately 15 mg of cellulose and pressed into a pellet. XAS data was measured in step scans between 40200 and 41423 eV.

## Data analysis

### *Reciprocal space refinement*

The analysis and processing of the ND data was performed by the Rietveld method [14] using GSAS and EXPGUI [15, 16]. This used Chebyshev polynomials to fit a background function and pseudo Voigt functions [17], convoluted with back-to-back exponentials to model the peak shape. This analysis allows combined refinement across all the detector banks.

### *Real space refinement*

The data correction for PDF used GUDRUN [18]. This normalises, merges data sets and corrects with respect to the vanadium containers and sample environment. The Fourier transformation of the $S(Q)$ data to calculate the $G(r)$ was performed using STOG [19] with $Q_{max} = 40\,\text{Å}^{-1}$ and a Fourier filter was applied with $r_{max} = 1.5$ Å to correct for a sloping background in the $S(Q)$.

### *XAS data correction and refinement*

The XAS data was normalised using EDA [20] software and underwent background subtraction for both K- and $L_3$-edge. A correction was required for the $L_3$-edge data to model a double excitation event at 5856 eV [21]. Ce $L_3$-edge XAS data was fitted between $k = 1.82$ and $9.26\,\text{Å}^{-1}$ and $r = 1.0$ and 2.70 Å. Ce K-edge was fitted between $k = 2.00$ and $14.10\,\text{Å}^{-1}$ and $r = 1.0$ and 5.5 Å. Amplitude reduction factor ($SO_2$) was set using ceria with a fixed coordination number of 8 for the first Ce–O path. $SO_2$ was set at 0.72 for the $L_3$-edge and 1.00 for the K-edge. Simultaneous combined edge analysis was performed to increase the number of shells that could be analysed. Artemis [22] was used to analyse the ($\chi(k)$) data to refine structural properties. Phase-shifts and amplitude factors were calculated with FEFF8l [23] using ceria fluorite crystallographic data. Hedin–Lundqvist potentials were used to calculate phase shifts and backscattering factors.

### *RMCProfile modelling*

The principle behind RMC is that a random atom within a configuration is moved a random amount away from its current position. The data associated with EXAFS and PDF can then be calculated and compared with experimental data sets, where fitting allows for calculation of an agreement function. RMC uses the Metropolis criterion to fit a model to multiple data sets allowing for short range, medium range and long range data to be modelled simultaneously. The Metropolis criterion, equation (1), is used to deduce whether a random move is accepted or rejected. A move that improves the fit, a negative $\Delta\chi^2$ will always be accepted. However there is also finite probability associated with the acceptance of a move that does not improve the fit, a positive $\Delta\chi^2$, compared with the

experimental data, however this is an exponentially decaying function limiting the probability of acceptance [24]

$$P_{\mathrm{RMC}} = \exp\left(\frac{-\Delta\chi^2}{2}\right). \quad (1)$$

This procedure however can result in multiple different structures being found with the simulation being run many times as the moves are random throughout. As a consequence of this, in the case of RMCProfile modelling each simulation was repeated 100 times. The analysis of the final results is then averaged over all simulations.

RMC simulations of all the ceria materials was accomplished using RMCProfile [19, 25]. This software can, simultaneously, perform modelling on both the Bragg diffraction and $G(r)$ data on a $6 \times 6 \times 6$ supercell. RMCProfile proceeds with the simulation by using an ideal crystal structure then moving each atom by a maximum amount of 0.05 and 0.10 Å for the Ce and O atoms respectively, with respect to the periodic boundary (where the cell is bordered by copies of itself) [24]. This will accept any move that improves the fit between experimental and calculated data. Further to this it will accept some moves that do not improve the fit in order to avoid being stuck in any local minima. The reciprocal space data is used by RMCProfile to constrain the crystallinity of the long-range structure whilst the $G(r)$ was modelled as two distinct data sets; one covering the range 1–5 Å and the second 1–15 Å, with the shorter range data being weighted 10-fold in comparison to the 1–15 Å.

Attempts were made to include EXAFS data into the RMCProfile fit but were unsuccessful due to software limitations, so EvAX was used to model the $L_3$- and K-edge EXAFS data.

### *EvAX modelling*

EvAX [26] is an RMC based modelling code that incorporates an evolutionary algorithm to search a large area of configuration space using a small supercell, in this case a $5 \times 5 \times 5$ supercell was used with a population of 32 used for the evolutionary algorithm. EvAX simulations were run 10 times to extract statistical errors. The evolutionary algorithm uses three operations: crossover, mutation and selection. Where a crossover operation is described as a genetic mixing of two configurations, a mutation involves the random moving of atoms within a configuration and the selection operation creates a new population from the old population of configurations with a weighted probability towards those with a high fitness value. The simulation also employs a simulated annealing approach, allowing for larger probability that moves are accepted at the start of the simulation with the criterion for acceptance becoming smaller throughout. In this manner the system reaches the global minimum in a computational efficient procedure. This procedure allows for unprecedented use of full multiple scattering calculations and fitting of higher order coordination shells, however due to the limitations on the $k$ range from the Ce $L_3$-edge this work has focused on the first two coordination shells.

During the modelling, Fourier transformed Ce $L_3$-edge data of the first shell, associated to the Ce–O distance, and

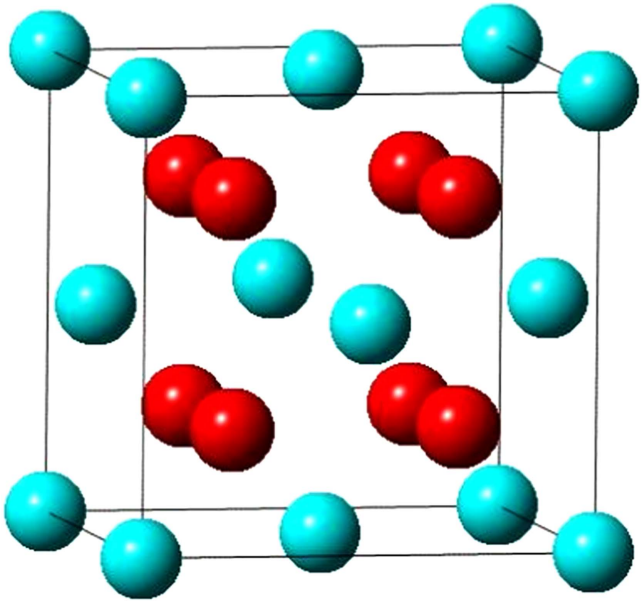

**Figure 1.** Ceria has the fluorite structure (space group: $Fm\bar{3}m$), Ce (Red): 4a, 0, 0, 0 and O (green): 8c ¼, ¼, ¼).

Fourier transformed Ce K-edge data of the first and second shells, associated mainly to the Ce–O and Ce–Ce distances, were used. This allows for modelling of the first and second coordination shells to be modelled jointly refining the atom positions in a real space configuration. The amplitude reduction factors were set accordingly from initial fitting undertaken on the $CeO_2$ NIST standard within the Athena/Artemis code [22] at 0.72 and 1.0 for the Ce $L_3$- and K-edges respectively. The $k$ range used during the fitting procedure was between 1.82 and 9.27 $Å^{-1}$ for the Ce $L_3$-edge and between 3.00 and 15.22 $Å^{-1}$ for the Ce K-edge. The fitting space used throughout the simulation was real space. A periodic boundary condition was employed starting from an initial ideal crystal structure.

## Results and discussion

$CeO_2$ has the fluorite structure (see figure 1) which has a crystal structure belonging to the space group $Fm\bar{3}m$, Ce(IV) ions occupy the 0,0,0 (4a) position and the oxygen atoms occupy 0.25, 0.25,0.25 (8c) position in the structure which has been well-established. Typical diffraction pattern of $CeO_2$ (x-ray and ND) data are shown in figure 2. First we discuss the use of RMCProfile method to determine the structure $CeO_2$ using ND data followed by the analysis of EXAFS data using EvAX.

### *Analysis of diffraction data using RMCProfile*

RMCProfile modelling was performed using a $6 \times 6 \times 6$ unit cell sized simulation box. This contained 864 cerium cations and 1728 oxygen anions. All the models assumed the materials were the stoichiometric fluorite structure as the input model, as suggested by our previously published extensive analysis using Rietveld, PDF methods and XAS on

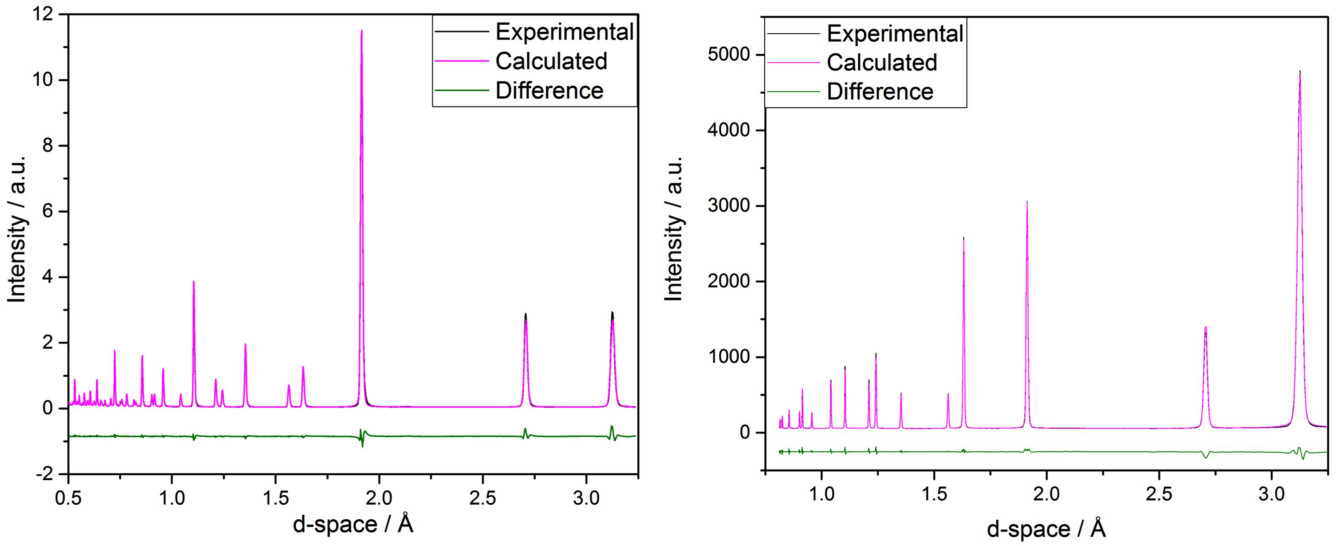


**Figure 2.** Comparison of experimental and calculated neutron diffraction patterns (left) and x-ray diffraction patterns (right) for the ceria sample derived from rietveld analysis.

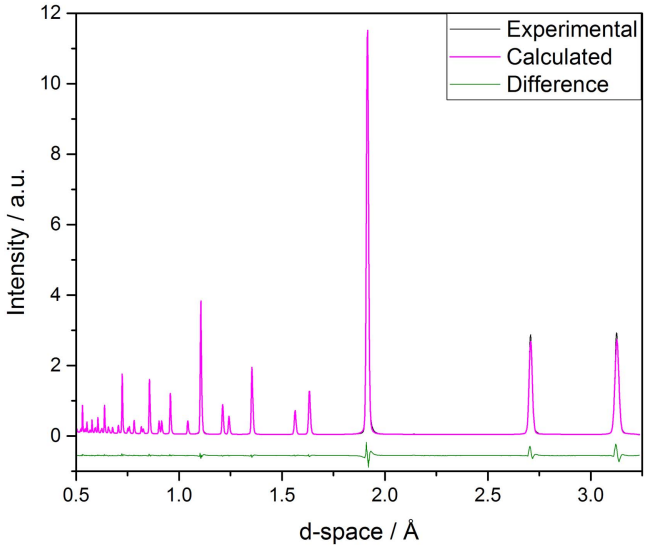


**Figure 3.** Comparison of the experimental and calculated bragg neutron diffraction patterns for ceria from RMCProfile.

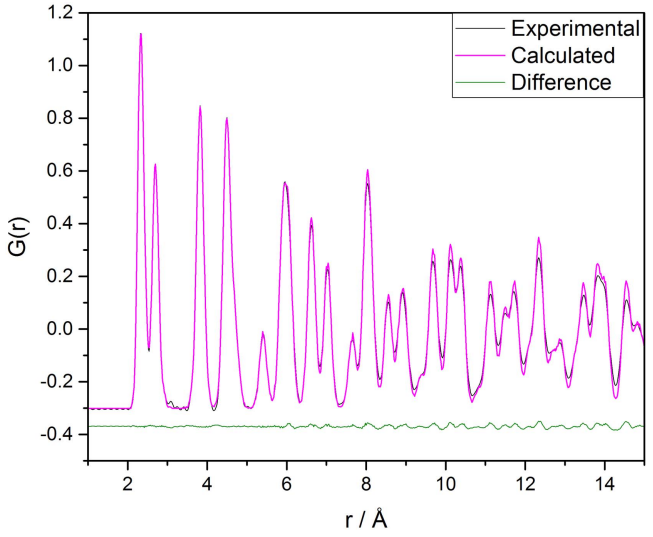


**Figure 4.** A comparison of experimental and calculated neutron $G(r)$ between 1 and 15 Å for ceria NIST from RMCProfile.

the same sample as described here [27]. In figure 3 we show the comparison of the diffraction data with that calculated based on RMCProfile analysis indicating very good agreement between the data and fit. In order to highlight the short and medium range structure, the $G(r)$ was separated into two distinct data sets, with one set fitting between 1–5 Å and another set fitting between 1–15 Å respectively. In figures 4 and 5 we show the best fit between experimental and calculated data using RMCProfile method, in particular highlighting the best match for short and medium range.

Our previously reported analysis of the ND and NPDF datasets individually show differing lattice parameters dependent on the technique used [27]. Analysis of the ND and NPDF data using the RMCProfile method successfully models these variations. This is performed by fixing the density to that refined by the Rietveld method for the supercell then allowing enough freedom for the model to account for the variations in pair correlations and lattice parameter across the short, medium and long range structure. This modelling shows that over these length scales the fluorite structure is observed. Furthermore with respect to the Bragg data the short range NPDF data is weighted more highly resulting in fitting of the low $R$ region more appropriately than achieved with equal weighting.

For comparison, all the supercells can be reduced down to a single unit cell, overlaying all the cerium and oxygen atoms. These representations, figure 6(A), show that the atoms are all offset from the ideal crystallographic positions, as expected due to the influence of thermal vibration.

Statistical analysis on the $6 \times 6 \times 6$ supercell was performed to give a histogram showing the radial distribution function around a central cerium cation. This gives a 1D representation of a 3D structure, figure 7(A). This shows that

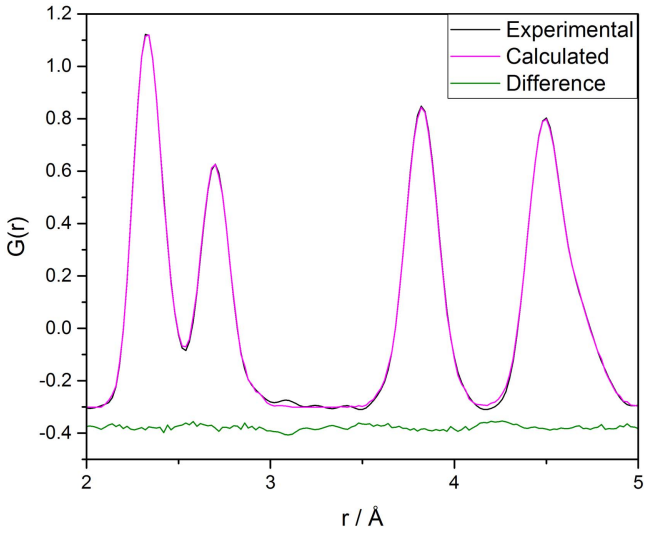


**Figure 5.** A comparison of the experimental and calculated neutron $G(r)$ between 1 and 5 Å for ceria NIST from RMCProfile.

the material is not a perfect crystal and the atoms are offset from their ideal site giving a range of interatomic distances.

Table 1 shows the associated bond angles for O–Ce–O and Ce–O–Ce respectively. For the O–Ce–O tetrahedral bond angle, we find that it is slightly disordered with respect to the ideal value of approximately 109.5°, figure 8 illustrates the bond angle distributions. This supports our previously published analysis indicating that ND, PDF and EXAFS show disordered atoms on the same sample material [27]. This discrepancy observed in both the differences with respect to both interatomic distances and interatomic bond angles is due to numerous effects. The comparison of the results obtained from Rietveld refinement and RMCProfile show that for both models there are relatively similar values seen with the exception of the Ce cubic angle. This can be explained by consideration of a random movement away from 180° resulting in the observed angle reducing as the direction of movement is not regarded, the inverse sine function always yields a result less than 180°. This comparison shows the similarities observed even though both are modelling the data in different manners, where the Rietveld is performed fitting one unit cell and the bond lengths/bond angles dependent on the lattice parameter and for RMCProfile there are no such symmetry constraints on the model and a supercell of $6 \times 6 \times 6$ unit cells is used. Figures 7(A) and (8) shows the comparison of the bond lengths and bond angles respectively derived from RMCProfile. The distribution of the values obtained from this are Gaussian like which indicates the isotropic disordering of the atoms present which coincides with that seen in the Rietveld refinement.

The mean square relative deviations (MSRD) have been calculated using equation (2) below where $R$ relates to the average interatomic distance for the correlation of interest, obtained through fitting a Gaussian to the RDF; $R_i$ represents the interatomic distance for a pair of atoms in the configuration. $N$ here is the total number of pair correlations considered

$$\frac{1}{N}\sum_i (R - R_i)^2. \tag{2}$$

The standard error is calculated through consideration of the standard deviation of the spread of the parameter of interest from each of the simulations conducted, equation (3). Here $N$ represents the total number of simulations, $\phi$ represents the mean value of the parameter of interest and $\phi_i$ represents the same interest parameter from each simulation

$$S = \frac{\sqrt{\frac{1}{N}\sum_i (\phi - \phi_i)^2}}{\sqrt{N}}. \tag{3}$$

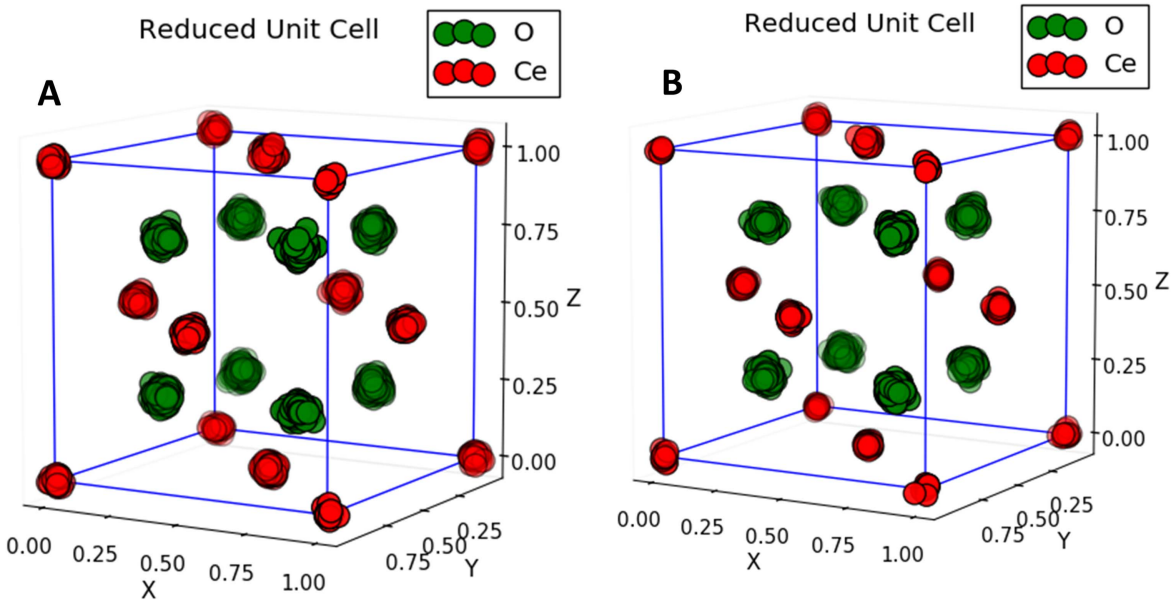


**Figure 6.** Reduced configuration to an overlaid single ceria unit cell derived from RMCProfile models combining neutron diffraction and pair distribution function data (A) and from EvAX models using joint Ce $L_3$ and K edge EXAFS data (B).

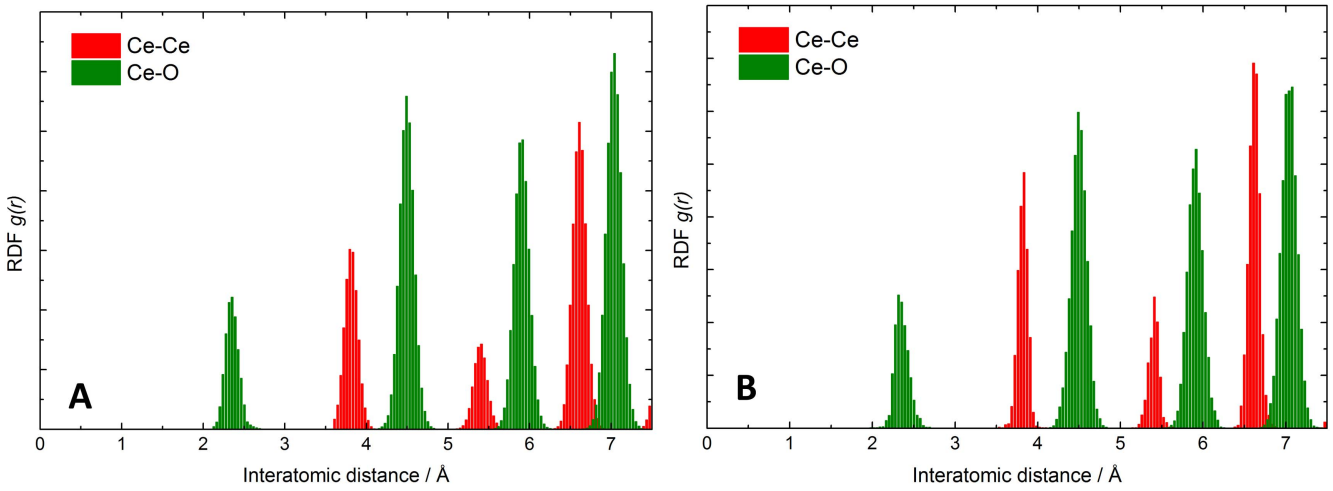


**Figure 7.** Histogram of the resultant radial distribution function around a central Ce atom for ceria NIST derived from RMCProfile combining Neutron diffraction and pair distribution function data (A) and EvAX modelling using Ce $L_3$- and K-edge EXAFS (B).

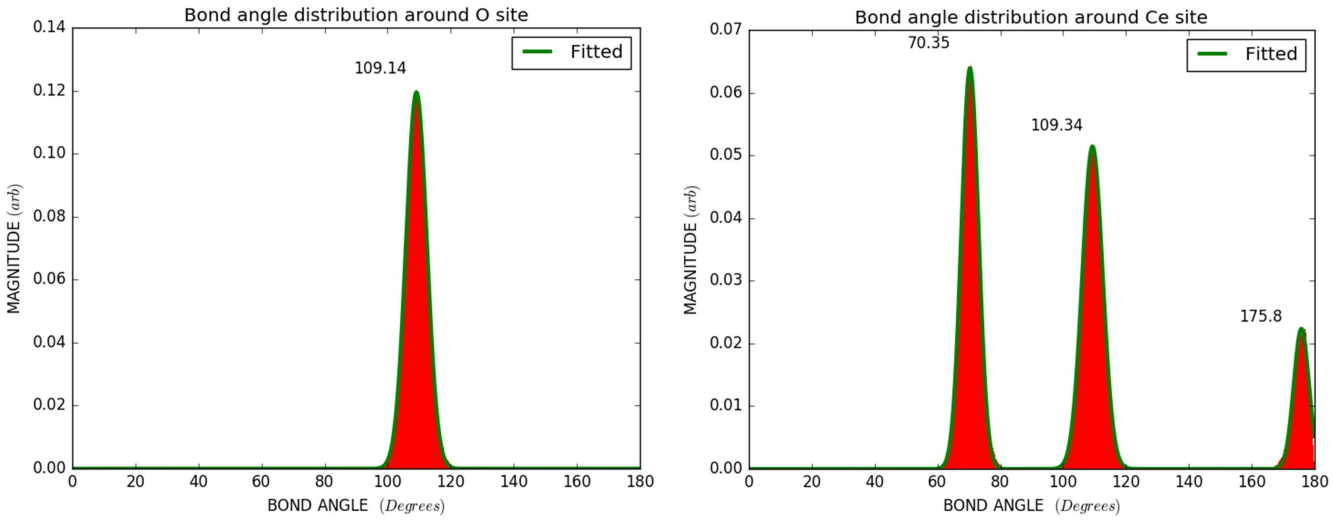


**Figure 8.** The respective O–Ce tetrahedral coordination and Ce–O cubic coordination derived from RMCProfile modelling.

**Table 1.** Calculated distances of atomic pairs and the relative mean square relative deviation from the final configurations produced in RMCProfile (top). Calculated bond angles associated to the oxygen and cerium coordination environments from the final configurations produced in RMCProfile (bottom).

| Atomic correlation | $R$ (Å) | Standard error (Å) | MSRD (Å$^{-2}$) | Standard error (Å$^{-2}$) | Rietveld $R$ (Å) | Rietveld error (Å) |
|---|---|---|---|---|---|---|
| Ce–O | 2.344 | $4 \times 10^{-5}$ | 0.006 77 | $1 \times 10^{-5}$ | 2.3431 | $1 \times 10^{-5}$ |
| Ce–Ce | 3.823 | $7 \times 10^{-5}$ | 0.006 60 | $1 \times 10^{-5}$ | 3.8262 | $1 \times 10^{-5}$ |
| O–O | 2.708 | $5 \times 10^{-5}$ | 0.007 86 | $1 \times 10^{-5}$ | 2.7055 | $1 \times 10^{-5}$ |

| | Angle (°) | Standard error (°) | Rietveld angle (°) |
|---|---|---|---|
| O tetrahedral bond | 109.14 | 0.003 | 109.47 |
| Ce cubic bond | 70.35 | 0.002 | 70.53 |
| | 109.34 | 0.002 | 109.47 |
| | 175.80 | 0.006 | 180 |

### *EXAFS data analysis using EvAX*

EvAX simulations using only experimental EXAFS data from the ceria sample have been carried out and show similar results to the RMCProfile refinement using ND and NPDF data. The fitting, in both $k$ and $R$ space EXAFS data, is shown in figure 9 for both the Ce $L_3$- and K-edge data showing good agreement of the simulation to the data. Calculations are performed on the best fitting configuration from the total

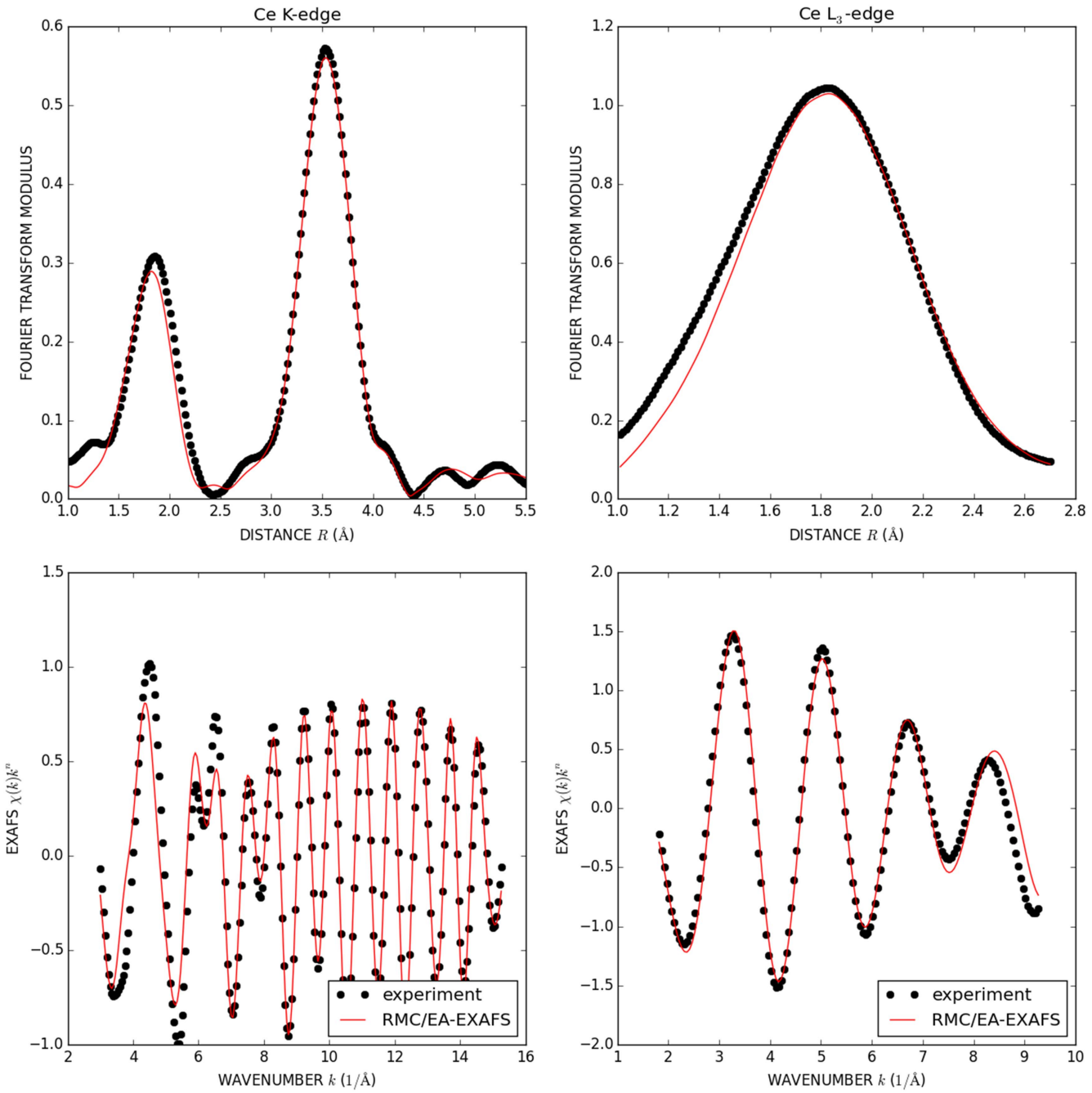


**Figure 9.** Fits shown for real space (top) and $k$ space (bottom) for the Ce K-edge (left) and Ce $L_3$-edge (right) respectively of the ceria NIST sample.

**Table 2.** Results for interatomic distances and mean square relative deviation for $CeO_2$ NIST EvAX simulation (top). Calculated bond angles associated with the oxygen and cerium coordination environments from the final configurations produced in EvAX (bottom).

| EXAFS path | $R$ (Å) | Standard error (Å) | MSRD (Å$^{-2}$) | Standard error (Å$^{-2}$) | Rietveld $R$ (Å) | Rietveld error (Å) |
|---|---|---|---|---|---|---|
| Ce–O | 2.3425 | $1 \times 10^{-4}$ | 0.0065 | $3 \times 10^{-4}$ | 2.3431 | $1 \times 10^{-5}$ |
| Ce–Ce | 3.8253 | $2 \times 10^{-4}$ | 0.0036 | $6 \times 10^{-4}$ | 3.8262 | $1 \times 10^{-5}$ |
| | Angle (°) | Standard error (°) | Rietveld angle (°) | | | |
| O tetrahedral bond | 109.12 | 0.010 | 109.47 | | | |
| Ce cubic bond | 70.25 | 0.005 | 70.53 | | | |
| | 109.22 | 0.006 | 109.47 | | | |
| | 175.77 | 0.008 | 180 | | | |

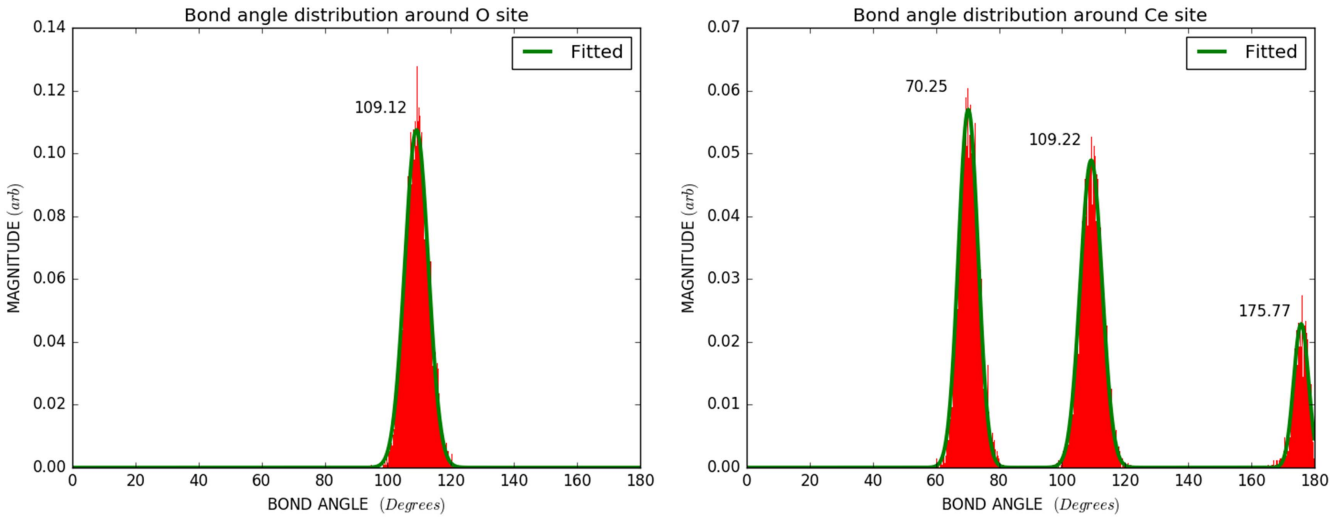


**Figure 10.** The respective O–Ce tetrahedral coordination and Ce–O cubic coordination derived from EvAX modelling for ceria NIST.

population. Figure 7(B) shows the resultant radial distribution function around absorbing Ce atoms in the total configuration derived from the EvAX modelling. It is evident that the O atoms between the layers of Ce atoms are disordered whereas the Ce atoms are well ordered on their crystallographic sites. Fitting results are shown in table 2 below. Figure 6(B) shows the reduced configuration to an overlaid single unit. This shows the atoms are all offset from the ideal crystallographic positions, as expected due to the influence of thermal vibration.

Table 2 shows that there is substantially more disorder within the O sites as compared to the Ce sites. This is in contrast to the RMCProfile modelling showing almost equal disorder. Whilst the RMCProfile simulations were carried out only using experimental data from Neutron experiments, the EvAX simulations were carried out only using XAS data. This illustrates the different sensitivity between the x-ray and neutron techniques towards differing element type. Therefore in future combining the x-ray and neutron datasets should be undertaken. However it should also be noted that that XAS is an element-specific local structure probe and due to the Ce absorption edge being used is centred upon a Ce atom unlike in the neutron total scattering experiments.

The calculated O–Ce–O tetrahedral and Ce–O–Ce cubic bond angles derived from the EvAX models are shown in table 2, with figure 10 illustrating the bond angle distributions. These values differ from the ideal values from a perfect crystal structure but similar to those seen from RMCProfile which indicates that models derived purely from EXAFS data suggest both cerium and oxygen are disordered. The agreement towards the Ce cubic bond angles between both RMCProfile and EvAX show that whilst EvAX is using data centred on the Ce site, RMCProfile is able to equally represent the disorder around the Ce site without the site specific local coordination environment information.

## Conclusion

Reverse Monte Carlo simulation analysis method was applied to diffraction, PDF and EXAFS ($L_3$ and K edges) of crystalline $CeO_2$ system. The analysis yielded some noticeable differences between the RMCProfile and EvAX simulation undertaken on *ex situ* ceria NIST sample such as variations in the atomic displacement parameters relating to the disorder around the Ce cubic site. We attribute this to the difference in sensitivity between the x-ray and Neutron based techniques towards the different elements, Ce and O. The models derived from RMCProfile modelling, combining ND and total scattering suggests that O–Ce–O and Ce–O–Ce bond angles are offset from the ideal structure due to disorder around these crystallographic sites, but that there are no drastic deviations from the ideal fluorite structure. The model obtained from EvAX analysis of the same sample again shows the fluorite structure. The refined interatomic distances and bond angles are offset from those for the ideal crystal structure indicative of some thermal or static disorder within the sample though more importantly showing that just using EXAFS for the model we can obtain an acceptable model in comparison to utilising short, medium and long range datasets obtained from neutron total scattering methodologies.

## Acknowledgments

We thank EPSRC and Johnson Matthey Plc for a Case Award (HRM and AHC). We thank the UK Science and Technology Facilities Council for allocating neutron beam time at the ISIS facility. We acknowledge the European Synchrotron Radiation Facility for provision of synchrotron radiation facilities. Computing resources were provided by STFC Scientific Computing Department's SCARF cluster.

## References


[1] Farrauto R J and Heck R M 1999 *Catal. Today* **51** 351–60
[2] Kašpar J, Fornasiero P and Hickey N 2003 *Catal. Today* **77** 419–49
[3] Trovarelli A 2002 *Catalysis by Ceria and Related Materials* (London: Imperial College Press)
[4] Trovarelli A, Leitenburg C D, Boaro M and Dolcetti G 1999 *Catal. Today* **50** 353–67
[5] Selvan V A M, Anand R B and Udayakumar M 2009 *ARPN J. Eng. Appl. Sci.* **4** 1–6
[6] Walton R I 2011 *Prog. Cryst. Growth Charact. Mater.* **57** 93–108
[7] Sears V F 1992 *Neutron News* **3** 26–37
[8] McMaster W H, Del Grande N K, Mallett J H and Hubbell J H 1969 *Lawrence Livermore National Laboratory, Report* UCRL-50174
[9] Mamontov E and Egami T 2000 *J. Phys. Chem. Solids* **61** 1345–56
[10] Hull S, Smith R I, David W I F, Hannon A C, Mayers J and Cywinski R 1992 *Physica* B **180–181** 1000–2
[11] Arnold O *et al* 2014 *Nucl. Instrum. Methods Phys. Res.* A **764** 156–66
[12] Nikitenko S, Beale A M, Van Der Eerden A M J, Jacques S D M, Leynaud O, O'Brien M G, Detollenaere D, Kaptein R, Weckhuysen B M and Bras W 2008 *J. Synchrotron Radiat.* **15** 632–40
[13] Mathon O *et al* 2015 *J. Synchrotron Radiat.* **22** 1548–54
[14] Rietveld H M 1969 *J. Appl. Crystallogr.* **2** 65–71
[15] Toby B H 2001 *J. Appl. Crystallogr.* **34** 210–3
[16] Larson A C and Von Dreel R B 1994 *Alamos National Laboratory Report* LAUR 86-748
[17] Thompson P, Cox D E and Hastings J B 1987 *J. Appl. Crystallogr.* **20** 79–83
[18] Soper A K www.isis.stfc.ac.uk/instruments/sandals/data-analysis/gudrun8864.html (accessed Oct 5, 2015).
[19] Keen D A, Tucker M G and Dove M T 2005 *J. Phys.: Condens. Matter* **17** S15
[20] Kuzmin A 1995 *Physica* B **208–209** 175–6
[21] Chaboy J, Marcelli A and Tyson T A 1994 *Phys. Rev.* B **49** 11652
[22] Ravel B and Newville M 2005 *J. Synchrotron Radiat.* **12** 537–41
[23] Ankudinov A L, Ravel B, Rehr J J and Conradson S D 1998 *Phys. Rev.* B **58** 7565–76
[24] McGreevy R L 2001 *J. Phys.: Condens. Matter* **13** R877
[25] Tucker M G, Dove M T and Keen D A 2001 *J. Appl. Crystallogr.* **34** 630–8
[26] Timoshenko J, Kuzmin A and Purans J 2014 *J. Phys.: Condens. Matter* **26** 55401
[27] Marchbank H R *et al* 2016 *Chemphyschem* **17** 3494-503